A Multi-Ion Permeation Mechanism in Neuronal Background Chloride Channels

FABIO FRANCIOLINI and WOLFGANG NONNER

From the Department of Physiology and Biophysics, University of Miami, Miami, Florida 33101

ABSTRACT Unitary current/voltage relationships of background Cl channels of rat hippocampal neurons were determined for varied gradients and absolute concentrations of NaCl. The channels revealed permeabilities for both Cl and Na ions. A hyperlinear increase of unitary conductance, observed for a symmetrical increase of salt concentration from 300 and 600 mM, indicated a multi-ion permeation mechanism. A variety of kinetic models of permeation were tested against the experimental current/voltage relationships. Models involving a pore occupied by mixed complexes of up to five ions were necessary to reproduce all measurements. A minimal model included four equilibrium states and four rate-limiting transitions, such that the empty pore accepts first an anion and then can acquire one or two cation/anion pairs. Three transport cycles are formed: a slow anion cycle (between the empty and single-anion states), a slow cation cycle (between the one- and three-ion states), and a fast anion cycle (between the three- and five-ion states). Thus, permeant anions are required for cation permeation, and several bound anions and cations promote a high rate of anion permeation. The optimized free-energy and electrical charge parameters yielded a self-consistent molecular interpretation, which can account for the particular order in which the pore accepts ions from the solutions. Although the model describes the mixed anion/cation permeability of the channel observed at elevated concentrations, it predicts a high selectivity for Cl anion at physiological ionic conditions.

INTRODUCTION

This paper continues an analysis of anion and cation permeability in neuronal background Cl channels. The preceding paper (Franciolini and Nonner, 1994) showed that the channel can conduct a wide variety of anions and cations including divalent forms and revealed violations of the Independence Principle that indicate interactions of anions and cations in the pore.

In this paper, the permeation of one salt, NaCl, is studied under varied gradients and absolute concentrations. The experimentally determined i/V relationships are

Address correspondence to Wolfgang Nonner, Department of Physiology and Biophysics, University of Miami, P.O. Box 016430, Miami, FL 33101.

Dr. Franciolini's present address is Istituto Biologia Cellulare, Universita di Perugia, 06100 Perugia, Italy.

J. GEN. PHYSIOL. © The Rockefeller University Press · 0022-1295/94/10/0725/22 $2.00
Volume 104 October 1994 725–746

used to develop a kinetic model of Cl and Na ion permeation. A multi-ion mechanism involving complexes of up to five ions (three Cl, two Na ions) can account for the observations, including a hyperlinear concentration dependence of unitary conductance. Model parameters are optimized to describe the measured i/V relationships and used to develop a molecular picture of the pore.

METHODS

The objective of the experiments was to determine unitary current/voltage (i/V) relationships of neuronal background Cl channels bathed in NaCl salines of varied concentrations. The preparation, experimental techniques, and analysis protocols have been described in the preceding paper (Franciolini and Nonner, 1994). In brief, Cl channel currents were recorded under voltage clamp from inside-out somatic membrane patches excised from cultured hippocampal neurons. The test salines contained the specified concentration of NaCl, 2 mM MOPS (3-[*N*-morpholino]propanesulfonic acid) buffer and 1 mM EGTA (ethylene glycol-bis(β-aminoethyl ether)*N*,*N*,*N'*,*N'*-tetraacetic acid) and were titrated with NaOH to a pH of 7.2. Unitary currents at particular voltages were determined by analysis of amplitude histograms. Voltages were corrected for electrode offsets and junction potential changes.

The following ionic conditions were examined (bath//pipette, in millimolar of NaCl): 75//150, 150//150, 300//150, 600//150, 1200//150; 75//300, 150//300, 300//300, 600//300, 1200//300; 300//600, 600//600, 1200//600. From one to five different bath (intracellular) salines were tested in each membrane patch, while the pipette saline remained constant. Temperature was maintained at 10°C. Theoretical calculations used ion activity coefficients equal to mean activity coefficients (Robinson and Stokes, 1965); activities of 59, 113.5, 213, 404, and 785 mM were used for the concentrations of 75, 150, 300, 600, and 1,200 mM, respectively.

Model optimizations were performed on averages of pooled i/V relationships in order to reduce the volume of computation. Since the corrections for electrode offsets varied among individual experiments, unitary currents measured for voltages within a 5-mV interval were interpolated and averaged about a median voltage.

Transport Models

Pore models were based on discrete reaction schemes, in which the pore assumes a limited number of relatively stable configurations that interconvert through configurations with shorter lifetimes. Whereas a discrete model with a manageable number of states can provide only an approximate description of a diffusionlike process in an aqueous pore, it is computationally simple and capable of mapping the stoichiometry and transport-limiting kinetic features of an underlying molecular process.

A pore configuration was characterized by the ensemble of ions present in the pore, the free energy required to create the configuration from the empty pore state under the standard condition (1 M, zero voltage, 10°C), and by the charge displaced when the ensemble of ions was moved into their positions through the intracellular pore mouth. This method of introducing the effect of electrical fields differed from the usual method, which assigns electrical distances to individual ion barriers and wells and considers ion–ion interactions in the form of repulsion factors. We used configuration charges because in a multi-ion configuration, individual ion positions cannot be determined unambiguously by model optimization. Ion interactions were expressed in the free energies of pore states. Both equilibrium and transitional configurations were parameterized in this way. Charges of transitional states either were treated as distinct free parameters, or were assigned the mean charge of the adjacent equilibrium states.

The computation of i/V relationships followed established methods (Hille and Schwarz, 1978; Begenesich and Cahalan, 1980). Rate constants were computed by scaling kT/h with Boltzmann factors that corresponded to the difference in total (basic and electrostatic) free energies between the transitional state and the starting equilibrium state. If in the transition an ion entered the pore through the extracellular mouth, the charge of the equilibrium state was augmented by the charge displaced in moving the ion to the intracellular side (because configuration charges were defined as if ions entered through the intracellular mouth). In some models, states interconnected by transitions with large rate constants were treated as being in thermodynamic equilibrium. A homogenous set of linear algebraic equations was established by writing expressions for the rate of change of the probability of each (kinetically distinct) pore configuration and equating these rates with zero as necessary for the steady state. The normalization condition (the sum of all state probabilities equals one) was substituted for one of the rate equations. The resulting inhomogenous system of linear equations was solved by Gaussian elimination, yielding the steady state probabilities of the different pore configurations. Ionic net transport rates were computed by determining the net traffic of each species through one of the pore mouths. These rates were scaled by the ionic charges and algebraically added to yield the ionic current.

The parameterization in terms of free energies and charges ensured that model optimizations by computer did not violate microreversibility or produce negative rate constants. For optimizations, configuration charges were mapped into logarithmic units according to $q = \ln[(Q - Q_{min})/(Q_{max} - Q)]$, where Q is the configuration charge and Q_{min} and Q_{max} delimit the range accessible for optimization. Ranges of configuration charges were restricted to the charges representing the extreme ion arrangements in the pore; e.g., for a configuration holding two anions and one cation, Q_{min} and Q_{max} were set to -2 and $+1$ elementary charges, respectively.

We formulated rate constants in terms of absolute rate theory because this conveniently constrained optimizations and simplified comparisons with the literature. The free-energy values associated with activated states are intended to serve as logarithmic measures of basic rate constants, but are not intended to characterize a physical 'activated state'.

The algorithms used in model optimizations are described in the Appendix.

RESULTS

Variations Due to Channel Heterogeneity

Fig. 1 shows i/V relationships determined for individual neuronal background Cl channels bathed in a variety of NaCl concentrations and gradients at 10°C. Each solid line drawn for a particular ionic condition refers to a separate membrane patch and represents the individual measurements of unitary current in the form of a fitted third-order polynomial (see Fig. 1 of Franciolini and Nonner, 1994). Superposition of these polynomials revealed the extent of heterogeneity between individual channels.

The largest number of i/V relationships ($N = 28$) was recorded with symmetrical 300 mM NaCl solutions, a reference condition used in many experiments (Fig. 1 *A*). The extremes of these individual i/V curves span a substantial range. At +30 mV, for instance, the currents had a standard deviation of 0.2 pA. This estimate is representative of the entire data set analyzed in this study: sampling and averaging of variances between -60 and $+60$ mV for the i/V curves of all 13 tested ionic conditions yielded an average standard deviation of 0.22 pA. This standard deviation

was used as a reference for judging residuals between experimental and theoretical *i/V* curves.

For comparison with theory, experimental *i/V* curves in subsequent figures are presented in the form of averages computed as described in Methods. Symbols in Fig. 1 plot such averages for comparison with the individual curves. Altogether, 65 *i/V* relationships recorded for 13 different combinations of internal and external NaCl salines were included in the analysis. Model parameters were usually determined through optimizations that considered this entire data set simultaneously (see Appendix).

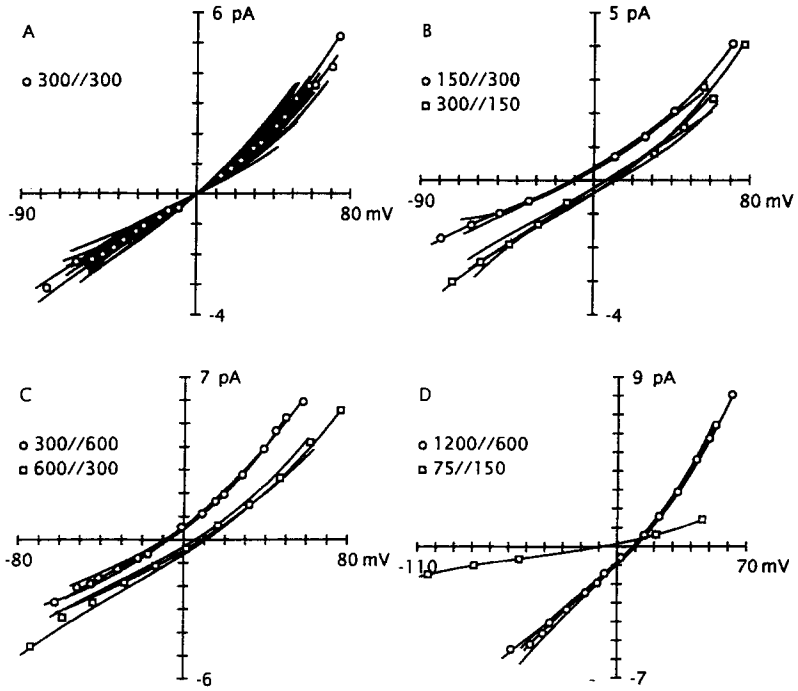

FIGURE 1. Unitary *i/V* relationships in NaCl salines at 10°C. (*A*) Symmetrical solutions; (*B–D*) 2:1 concentration gradients (indicated as internal//external). (*Solid lines*) Third-order polynomials fitted to measured unitary currents; each *i/V* curve represents a different membrane patch. (*Symbols*) Mean currents determined by averaging the measurements of unitary currents (see Methods).

Basic Models of Anionic and Cationic Conduction and Comparison with Data

Fig. 1, *B–D*, shows *i/V* curves recorded with 2:1 NaCl gradients of varied direction and absolute concentration. In all cases the zero-current potential was significantly smaller than the chloride equilibrium potentials calculated for the respective activity ratios (15.5–16.2 mV). This result conforms with previous observations (Franciolini and Nonner, 1987, 1994; Blatz, 1991), which demonstrated that neuronal background Cl channels pass alkali and organic cations. The magnitude of the zero-

current potentials varied little with the direction of the gradient or absolute salt concentration in the range of 150–1,200 mM. Experiments with larger NaCl gradients, summarized in Fig. 2 (*symbols*), gave analogous results.

The *i/V* curves in Fig. 1 exhibit outward rectification and superlinearity. The rectification is intrinsic rather than of the Nernst-Planck type because it is not reversed upon a reversal of the ion gradient (Fig. 2, *B* and *C*). The superlinearity suggests that substantially voltage-dependent rates are limiting ion permeation. These properties indicate that interactions with the pore impose significant constraints on ion permeation in this channel.

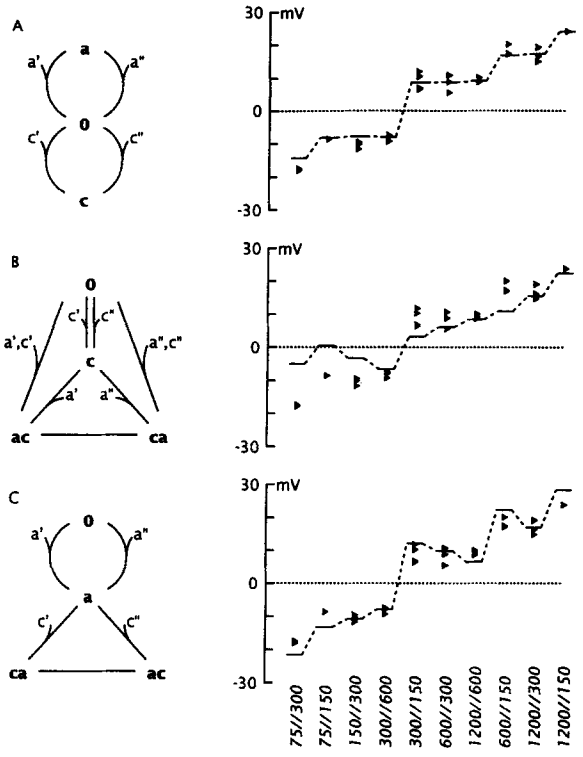

FIGURE 2. Zero-current potentials of three basic permeation models. In the kinetic schemes (*A–C, left*), pore states (*boldfaced*) are denoted by indicating the ions present in the pore (*c*: cation; *a*: anion; *0*: no ion); in schemes *B* and *C*, two different orientations of an ion pair are distinguished (*ac* and *ca*). Ions exchanged between the pore and the intracellular (extracellular) bath are shown on the left-hand (*right-hand*) side of reaction paths and marked by a single (double) apostrophe. The experimental zero-current potentials for 10 different NaCl gradients are plotted as symbols and compared with the theoretical zero-current potentials of each model (*lines*). These were computed using the model parameters (Table I) determined by fitting each model to all experimental *i/V* relationships.

In developing a transport model that could account for these features we first tested basic schemes that represented prototypes of alternative mechanisms. Our approach was to fit these models to the entire set of *i/V* curves, to use the parameters thus determined to predict crucial experimental observations, and then test the predictions in order to identify the most useful scheme.

Three basic pore state diagrams are shown at the left of Fig. 2. In Scheme A, Na and Cl ions move through the same pore, but do not dwell in the pore simultaneously. Hence, Na and Cl permeation are minimally interdependent. Scheme A

would apply to a pore whose walls bear no significant electrostatic charge or carry dipolar charges that can interact with ions of either polarity. Schemes B and C represent pores that have an innate preference to associate either with Na or with Cl ion, and in the associated form become accessible to the other ion. This mechanism could involve a fixed charge located in the pore or near the pore mouths. In Scheme B, Na ion binds to the pore and while bound promotes the permeation of Cl ion. Na ion can permeate individually or travel in the form of an ion pair. This specific scheme was proposed by Franciolini and Nonner (1987). In the converse, Scheme C, the pore primarily accepts and passes Cl ion; a bound Cl ion, however, also can allow Na ion to permeate. This scheme was used by Borisova, Brutyan, and Ermishkin, (1986) to account for zero-current potentials of amphotericin B pores, and, in a form involving several fixed charges in the pore lining, was proposed by Zambrowicz and Colombini (1993) for the VDAC pore.

Model parameters obtained by optimizations of these models are listed in Table I. The residuals between experimental and theoretical curves were similar for all schemes, three to four times larger than the minimal variance expected from channel heterogeneity. Optimizations started from varied initial parameters converged to virtually indistinguishable theoretical i/V curves.

Fig. 2 (*right*) compares zero-current potentials determined for a range of NaCl gradients (*symbols*) with those predicted by the three basic models (*lines*). The zero-current potential for a given concentration ratio is expected to be constant under varied absolute concentrations if Cl and Na ions cross the channel independently of each other, and indeed, Scheme A was in reasonable agreement with the observed zero-current potentials. In Schemes *B* and *C*, binding of the primary ion species conditions the pore for conducting the other species, so one would expect the Na/Cl permeability ratio to vary with absolute salt concentration. In fact, this is borne out. Scheme B yields fair agreements with large concentrations (e.g., 1200//300), but gives zero-current potentials of smaller magnitude, or even different polarity, than observed with low salt concentrations (e.g., 75//150), where the model becomes a cation conductor. Scheme C reproduces the zero-current potentials more accurately, albeit the concentration-dependent variations are larger than those observed. The comparison of zero-current potentials thus favors Schemes A or C over B. The good agreement of Scheme A might suggest that Na and Cl ions permeate independently of each other. However, improved versions of Scheme C considered below also produce an approximately constant Na/Cl selectivity over a range of concentrations (Fig. 8 *A*).

The various basic models also make different predictions concerning whether the channel can conduct cations unaccompanied by anion: Schemes A and B predict that Na current can be observed when Cl is unavailable as a charge carrier, whereas Scheme C predicts that in the bilateral absence of permeant anions there can be no measurable cation current, because the presence of anion is required for cation permeation. Franciolini and Nonner (1987) found no inward (outward) current after replacement of intracellular (extracellular) Cl by impermeant sulfate (their Fig. 10 *A*), and no measurable current at all following bilateral replacement of Cl by sulfate (their Fig. 10 *B*). The absence of directly observable Na currents supports model C,

TABLE I

Parameters of Permeation Models

Model A			Model B			Model C			Model D			Model E		
	kT	*e*		*kT*	*e*		*kT*	*e*		*kT*	*d*		*kT*	*e*
S1	4.40	−0.38	S1	−2.88	0.05	S1	3.39	−0.54	S1	−0.14	−0.56	S1	−1.23	−0.56
S2	1.53	0.09	S2	1.44	−0.20	S2	0.75	−0.73	S2	3.69	0.00	S2	−2.92	−0.27
T01′	11.96	−0.19	S3	1.29	0.08	S3	0.53	−0.86	S3	1.74	0.00	S3	−5.08	0.29
T01″	11.13	−0.69	T01′	10.81	0.02	T01′	11.97	−0.27	S4	−2.31	−0.38	T01′	11.89	−0.23
T02′	11.80	0.04	T01″	11.84	0.52	T01″	10.77	−0.70	T01′	11.05	−0.28	T12′	6.53	−0.21
T02″	13.35	0.54	T12	7.66	−0.11	T12′	8.21	−0.70	T01″	11.30	−0.78	T12″	9.89	−0.13
			T13	8.87	−0.51	T13″	12.35	−0.20	T12′	10.55	0.28	T23″	7.26	0.13
			T23	8.26	−0.09	T23	7.79	−0.81	T13″	11.51	−0.22			
			T02	11.34	−0.13				T23	3.90	0.00			
			T03	9.33	−0.05				T24′	3.63	−0.19			
									T34″	10.34	−0.69			

The free energies (in kT) and charges (in electron charges) of the equilibrium states (S) and transition states (T) were determined by a simultaneous least-squares fit of all experimental i/V relationships (models *A, B, C, E*) or of relationships obtained with symmetrical salines (Fig. 5 *A*, model *D*). In models *A–C*, transition state charges were set halfway between the fitted charges of the adjacent equilibrium states. In all schemes, states are numbered from top to bottom (no parameters are listed for the reference state S0), then left to right. For example, for model *D* (Fig. 5): S0-0 (no ions in pore); S1-a (one anion in pore); S2-ca (one anion, one cation; cation facing internal side); S3-ac (one anion, one cation; cation facing external side); S4-aca (two anions, one cation). Transition states are labeled in addition by single or double apostrophes, which indicate the side of ion exchange (intra- or extracellular, respectively). For example, for model *D:* T01′ = transition between S0 and S1 by accretion/release of anion through the intracellular mouth; T34″ = transition between S3 and S4 by accretion/release of anion through the extracellular mouth.

but the possibility remains that the currents of interest were not observed because the channels did not open under the conditions of the tests.

Fig. 3 *A* shows data from a previous experiment (Franciolini and Nonner, 1987; their Fig. 10 *C*) to resolve this issue: here Na_2SO_4 was added to (rather than substituted for) internal NaCl, and produced virtually no effect on zero-current potential or current amplitudes. Model A (Fig. 3 *B*) predicted a marked change in the zero-current potential, and a small increase in outward current. Model B (Fig.

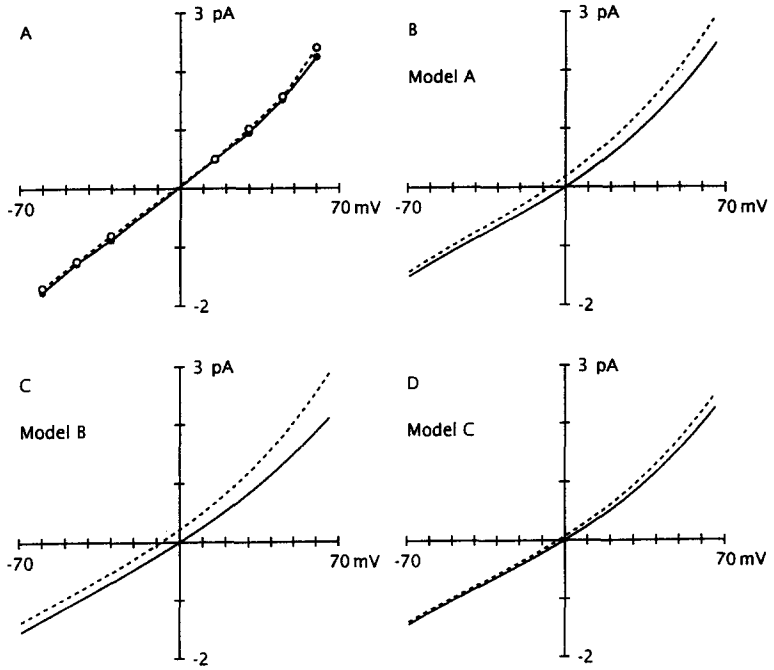

FIGURE 3. Experimental and theoretical *i/V* relationships for Na_2SO_4-addition experiment. (*A*) *i/V* relationships recorded in symmetrical 150 mM NaCl salines (*filled circles*) and following addition, to the internal 150 mM NaCl saline, of 100 mM Na_2SO_4 (*open circles*). Data from Franciolini and Nonner (1987, their Fig. 10 *C*). (*B–D*) Theoretical *i/V* relationships computed with models *A*, *B*, and *C*, respectively. Solid lines refer to the symmetrical 150 mM NaCl salines, the dashed lines, to the condition after internal Na_2SO_4 addition. The experimental data in *A* were obtained at 25°C; model parameters were determined from records at 10°C. Model C (*D*) most accurately predicts the very small observed effects of Na_2SO_4 addition.

3 *C*) predicted a change of zero-current potential and a larger increase in outward current, because at positive potentials the elevated internal cation concentration increased outward cation flux, and in addition promoted inward anion flux (by increasing cation occupancy of the pore). These large predicted changes were well within the range of detection, yet no such changes were seen. Model C (Fig. 3 *D*) most correctly predicted the small size of the effects of Na_2SO_4 addition: as cations

dwelled in the pore more frequently, they prevented anion from leaving the pore, so the increase in cation efflux was partially balanced by a decrease in anion influx.

The results of ion substitution experiments presented in the accompanying paper (Franciolini and Nonner, 1994) provide further arguments against mechanisms A and B. First, bilateral substitution of Na ion in symmetrical 300 mM salines by organic cations (e.g., triethanolamine) had no appreciable effect on unitary current magnitudes. A pore conforming to model B, in which a bound bulk cation catalyzes anion flux, would be expected to reveal significant conductance changes if a small alkali cation like Na is substituted by a large organic cation. Second, substitution of Cl by permeant anions of different permeabilities (e.g., NO_3, F) in salt gradient experiments produced very small, if any, changes of zero-current potential (cf. Figs. 5 and 6 in Franciolini and Nonner, 1994). This result indicates a significant interaction of anion and cation fluxes and differs markedly from the prediction of model A that substitution of Cl with anions of different permeabilities should result in substantial variations of the zero-current potential and the cation-anion permeability ratio.

In summary, of the three basic models tested, Scheme C (Borisova et al., 1986) appears to be the most appropriate: the pore per se conducts anion, but an anion dwelling in the pore can mediate cation conduction. Refined versions of Scheme C are considered below.

Multi-Ion Pore Models

Optimizations of basic models A–C did not yield the smallest residuals that could be expected. In fact, these basic models accounted poorly for the current amplitudes observed under certain ionic conditions. For example, the symbols in Fig. 4 plot experimental i/V curves obtained with symmetrical NaCl solutions of three concentrations. The relationship for 300 mM was fitted with a third-order polynomial. This curve was scaled by the activity ratio for comparison with the results at 150 and 600 mM. The experimental currents increase nearly proportionally between 150 and 300 mM, but in a hyperlinear fashion between 300 and 600 mM.

The hyperlinear concentration dependence indicates that conduction in the Cl channel pore is a cooperative high-order process, involving interactions of two or more ions with the pore. Furthermore, these ions must have similar affinities for the pore or affinity may even increase with the number of ions bound.

If the Cl channel were to admit anions exclusively, one would expect the electrostatic repulsion among the ions to result in widely separated apparent dissociation constants. Postulated 'repulsion factors' (Hille and Schwarz, 1978) tend to be large even among monovalent ions. For instance, Naranjo and Latorre (1993) estimated that in Na channels adsorption of a first Na ion to the pore, which has two sites with identical dissociation constants, increases the apparent dissociation constant for the other site from 18 mM to 47 M. Hence, any conductance increases due to successive acquisitions of ions would occur in the form of widely spaced first-order isotherms. Interaction of permeating anions with positive fixed charges near the pore mouths would have an analogous effect: bulk concentration changes would be attenuated into subproportionate changes of anion concentration at the pore mouths, and thus, would work against a hyperlinear concentration dependence of anion current (see, e.g., Naranjo, Latorre, Cherbavaz, McGill, and Schumaker, 1994).

On the other hand, hyperlinear characteristics could be expected if the channel admits both polarities of ion. Here, association of an ion of one polarity could greatly enhance the association of an ion of the opposite polarity. It is conceivable that additional ions could be accommodated in an alternating order, and that certain forms of such multiple occupancy might support particularly high rates of ion permeation. A cooperative effect of this kind could produce the observed hyperlinear concentration dependence of unitary current.

Ions diffusing through such a pore are unlikely to move in a single file along a linear chain of preformed binding sites. An ion may associate with 'sites' transiently formed by other mobile ions, and these ion arrangements may become polarized and oriented in numerous fashions by the electric field. We therefore did not attempt to divide the pore geometrically into ion barriers and wells, nor did we introduce the single-file restriction. Instead, pore states were defined in terms of the ensemble of ions present in the pore and further distinguished by their basal (zero-voltage) free energy and their electrical charge as indicated in Methods. The charge of a pore state is the charge displaced when the ensemble of ions is introduced into the pore through the intracellular mouth and allowed to organize itself in the state-specific form.

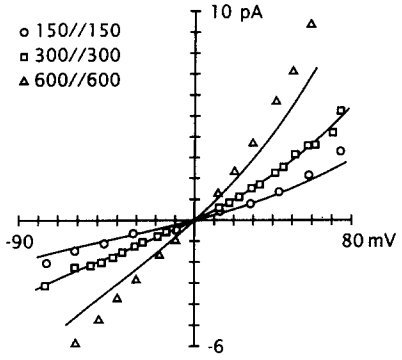

FIGURE 4. Concentration dependence of unitary currents. Experimental i/V relationships (*symbols*) were determined in symmetrical NaCl salines of three different concentrations. The currents obtained in 300 mM (*squares*) were fit by a third-order polynomial (*middle line*). The other curves were obtained by scaling this polynomial with the salt activities. Increasing the concentration from 300 to 600 mM leads to a larger than proportional increase in unitary currents.

A complex of two ions was considered in basic Schemes B and C (Fig. 2). Scheme C, the more suitable alternative, did not express hyperlinear conductance characteristics when configured to reproduce the relatively small cation permeability: the reactions involving the anion/cation complex were relatively slow, such that bound cations exerted a mild block. Therefore, a triple or higher occupancy is required for a scheme of this kind to explain both cation permeation and the hyperlinear concentration characteristics seen in Fig. 4.

Scheme D in Fig. 5 exemplifies a pore that can accommodate an anion-cation-anion complex. This model reproduced the experimental i/V curves in symmetrical salines very accurately (Fig. 5 *A*) when it was optimized for this subset of measurements. However, if the same parameters were used to predict i/V relationships obtained with a 1,200-mM internal NaCl solution, this model yielded currents substantially larger than those observed (Fig. 5 *B*). The hyperlinear increase of current thus, did not extend to 1,200 mM, which could indicate the beginning of

saturation or self block. When the model was allowed to adjust in this direction using an optimization involving the full set of experimental i/V curves, the residuals became more balanced, but substantial differences remained at both the lowest and highest concentrations. This three-ion model thus accounted only partially for the concentration dependence of the experimental i/V relationships, indicating that the actual mechanism was of higher than third order.

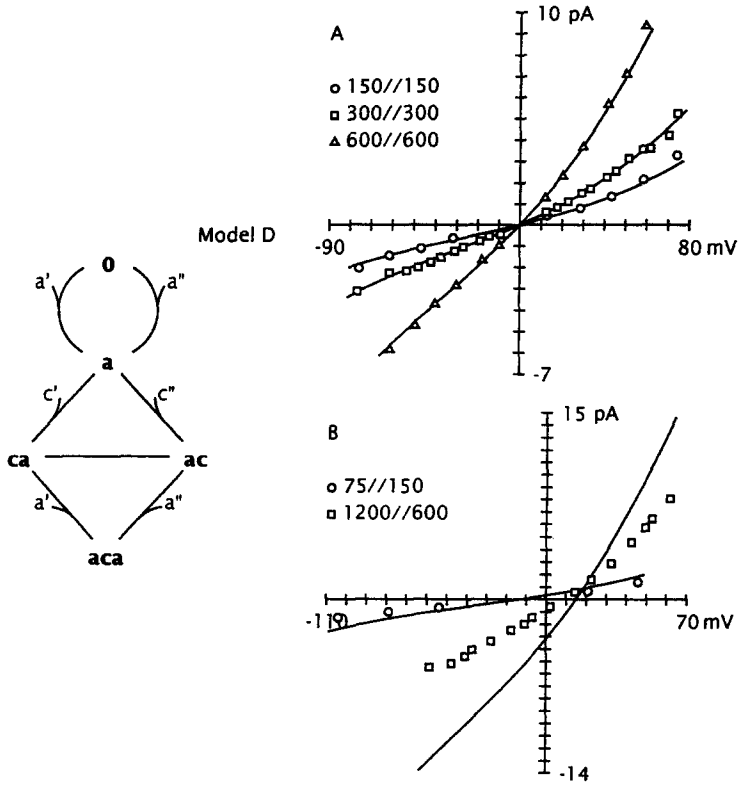

FIGURE 5. A three-ion pore model partly predicts the concentration dependence of unitary currents. (*A*) Experimental i/V relationships for three symmetrical conditions (*symbols*) were fitted using model *D* (*curves*). (*B*) Experimental i/V relationships obtained for two other ionic conditions are compared with those predicted from model *D* using the parameters from the fit in *A* (listed in Table I). Model *D* cannot fit the observed combination of hyperlinear and saturating concentration effects.

Models of such order become increasingly complex. We screened 47 versions in order to elucidate essential features. The five-ion (three-anion, two-cation) model E diagrammed in Fig. 6 summarizes the results in a minimal form. This model accounts well for the experimentally observed i/V relationships (Fig. 7) and zero-current potentials (Fig. 8 *A*) of this study, and gives correct predictions (Fig. 8 *B*) for the sulfate substitution/addition experiments of Franciolini and Nonner (1987). The i/V relationships were fit with an average residual of 0.2 pA, indicating that the

remaining differences were statistically indistinguishable from variations due to channel heterogeneity.

Model E provides two transport cycles for anion and one for cation. The single-anion cycle, which prevails at low ion concentration, has a slower rate than the multi-ion cycle prevailing at high concentrations. The intermediate cycle that transports cations requires bound anions to proceed. Although two cycles involve movements of several ions, all cycles deliver one anion or one cation per revolution. The model parameters (Table I) imply that half-saturation of the one-, three-, and five-ion states occurs at activities of 288, 377, and 360 mM, respectively.

The following features were determined to be necessary for predicting the experimentally observed i/V curves: (*a*) following binding of the first anion, stable configurations occur after the accretion of one or two cation/anion pairs. This rule was plausible because it maintained electroneutrality. It was instrumental for generating the observed steep concentration dependence of unitary current. Optimizations of other models that included states with intermediate numbers of bound ions typically assigned low levels of occupancy to such states, making them indistinguish-

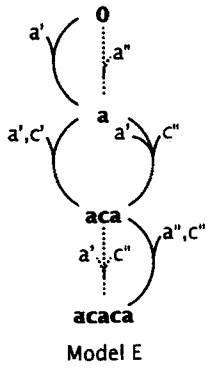

FIGURE 6. A five-ion permeation model. The solid lines in the scheme indicate pathways whose rate constants were determined by fit; dashed lines represent pathways along which virtual equilibria are maintained. The scheme has been reduced to states of significant occupancies; thus several reactions involve the simultaneous exchange of two ions. The optimized model parameters are listed in Table I.

able from transition states. The free energies determined for the two-ion states (S2, S3) of model D (Table I) exemplify this feature.

(*b*) Each ion-transporting cycle is rate limited by a single transition. After optimization other transitions of a cycle had rates sufficiently rapid to result in a virtual equilibrium between the adjacent states. In model D, for instance, when the parameters concerning the high-order anion transport cycle (involving states *ca, ac,* and *aca* in Fig. 5) were optimized two of the transition states (T23, T24′) received free energies ~6 kT smaller than that of the third (T34′; Table I). Equilibrium approximations have therefore been incorporated into the anion-transporting cycles of Scheme E and are de facto established by the rate constants of the cation-transporting cycle: one of these transitions (T12′) is the most rapid (nonequilibrium) transition retained in the model.

The reason that model optimizations generated such disparate rate constants becomes apparent if one considers the voltage dependence of the unitary current. Even at elevated concentrations, when the pore is likely to contain several ions, both the negative and positive branches of i/V curves were hyperlinear. The combined

equivalent charges required to account for this voltage dependence equaled about one electron charge. In a multi-ion pore, the equivalent of one large charge displacement can occur via smaller displacements of several ions if these occur in concert rather than in kinetically distinct individual movements. To allow one transition to assume the effective voltage dependence of one electron charge, any other rate in the cycle had to be sufficiently large that it never became rate limiting. Alternative models that achieved the required voltage dependence by transporting more than one ion per cycle (e.g., one cation against one anion) were found to be inconsistent with the experimental zero-current potentials.

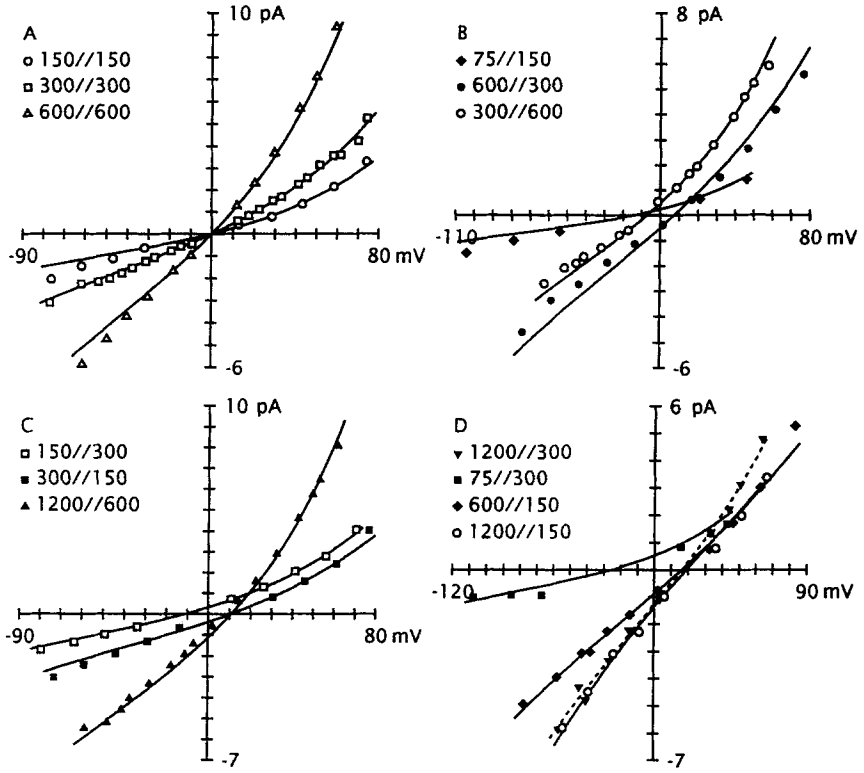

FIGURE 7. Experimental i/V relationships (*symbols*) and theoretical i/V curves (*lines*) of model E (whose scheme is shown in Fig. 6). The theoretical curves were obtained by a simultaneous fit of all experimental relationships with one set of parameters (listed in Table I).

(*c*) The model balances the effects of voltage and ion concentrations on the occupancies of multi-ion states. This was necessary for reproducing the experimental i/V curves recorded for different absolute concentrations and gradient directions (Fig. 7). In Scheme E, the virtual equilibria between lower and higher states involve ions that are alternately or simultaneously recruited from both bulk solutions. The order in which rapid reactions allow ions to enter the pore in Model E implies also a balanced succession of charge increments, such that the occupancies of multi-ion

states do not become strongly dependent on voltage. A number of models that involved a different order of ion entries reproduced the experimental i/V relationships as well as model E, but required implausible charge parameters to achieve a good fit. Specifically, all of these models required a four- or five-ion state in which all cations were grouped near one mouth of the channel while the anions were concentrated near the other.

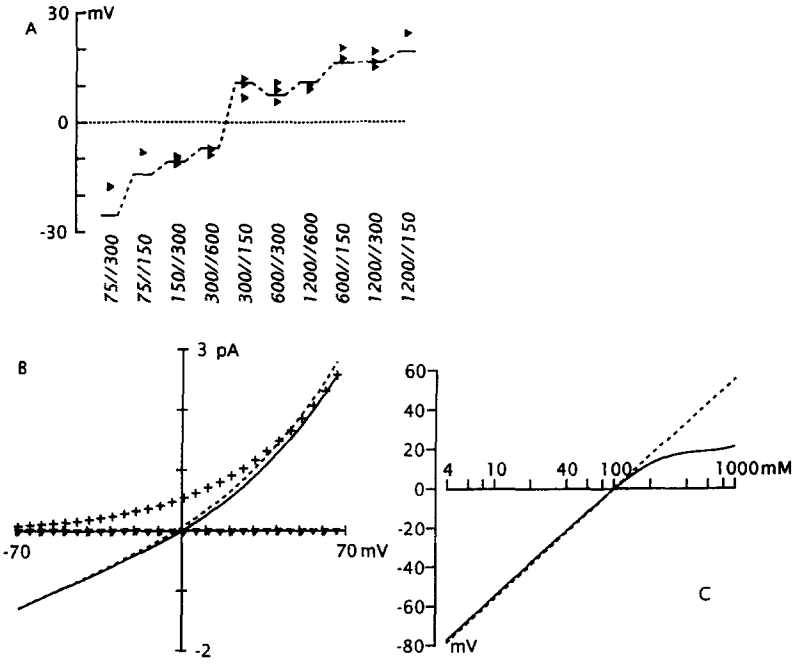

FIGURE 8. Predictions of model *E*. (*A*) Experimental (*symbols*) and theoretical (*lines*) zero-current potentials (compare to Fig. 2). (*B*) Predicted i/V curves for sulfate addition/substitution experiments: 150 NaCl//150 NaCl (millimolar, ext//int, *solid line*), 150 NaCl//100 Na_2SO_4 (*crosses*), 100 Na_2SO_4//100 Na_2SO_4 (*triangles*), and 150 NaCl//(150 NaCl + 100 Na_2SO_4) (*dashed line*). (*C*) Prediction of the zero-current potential for Cl substitution and salt-gradient experiments. The external NaCl activity was constant at 100 mM. The negative zero-current potentials were calculated for isosmotic internal solutions in which a varied fraction of NaCl was substituted by the Na salt of an impermeant anion. The positive zero-current potentials were calculated for a salt-gradient experiment in which the NaCl activity of the internal saline was increased from 100 mM up to 1 M. The solid line represents the zero-current potential of model *E* versus the internal Cl activity, the dashed line, the Nernst potential for Cl. The model predicts a sharp transition from the behavior of a virtual Cl electrode (when internal Cl activity is below 100 mM) to the behavior of an electrode with limited cation/anion selectivity (when internal NaCl activity is higher than 100 mM).

A molecular interpretation of model E is presented in the Discussion. Because the interpretation relies on fitted parameter values, we sought to determine confidence limits for these parameters. Fig. 9 shows scatterplots of the free energy of each state versus the charge of the state. The plotted parameter values were obtained from two

sets of repeated optimizations. Fig. 9 *A* represents results obtained using randomized initial parameters and the full set of experimental observations. For all states but one, all 20 fits converged to closely similar parameter values. The only weakly defined state was transition state T12′, in the faster of the two reactions of the cation transporting cycle. Fig. 9 *B* plots results from a Monte Carlo bootstrap simulation (see Appendix). Here synthetic data sets were created by random drafts with substitution from the original data set and used for parameter optimizations. Again, the scatter among the 20-parameter determinations is sufficiently small to define pore charges within ~0.1 e, and free energies within 1 kT U.

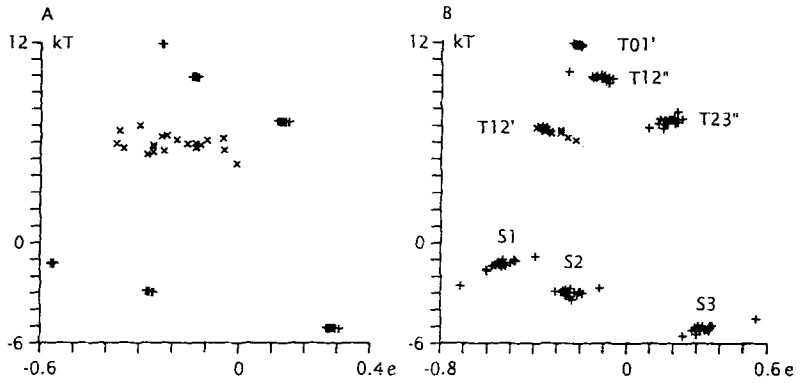

FIGURE 9. Confidence limits for the parameters of Model E. (*A*) Scatterplot of parameter values obtained by 20 model optimizations, each of which started from a randomly modified set of initial parameters (energies were varied between −kT and kT from those given in Table 1 for model E; charges (in their logarithmic form, see Methods) were varied by adding random values between −1 and +1. (*B*) Scatterplot from model optimizations on 20 complete data sets randomly selected from the original set (see Appendix). Each cluster represents empirical distributions of the free energy and charge parameters of a state. (*x*): transition state T12′ (revealing the widest scatter). Other states (+): equilibrium states S1, S2, and S3 (negative free energies, from left to right), and transition states T01′, T12″, and T23″ (positive free energies, from top to bottom).

DISCUSSION

Measurements of zero-current potentials have shown that both anions and cations can contribute to the unitary currents through neuronal background Cl channels and have revealed interactions between anions and cations in the pore. The new observation that unitary current amplitudes increase in a hyperlinear fashion over a range of NaCl concentrations led us to consider mechanisms in which the presence of several anions and cations in the pore promotes ionic current. A kinetic model developed on this basis satisfactorily predicts the i/V relationships recorded in various concentrations and gradients of NaCl and Na_2SO_4. We now use this model to outline a molecular picture of the pore.

A Molecular Interpretation of the Permeation Model

The best-fitting five-ion kinetic model developed in Results (Fig. 6, Table I) was reduced to pore states that are significantly occupied and to transition states associated with rate-limiting steps. The retained features are sufficiently well defined (Fig. 9) to support a molecular interpretation, such as that illustrated in Fig. 10.

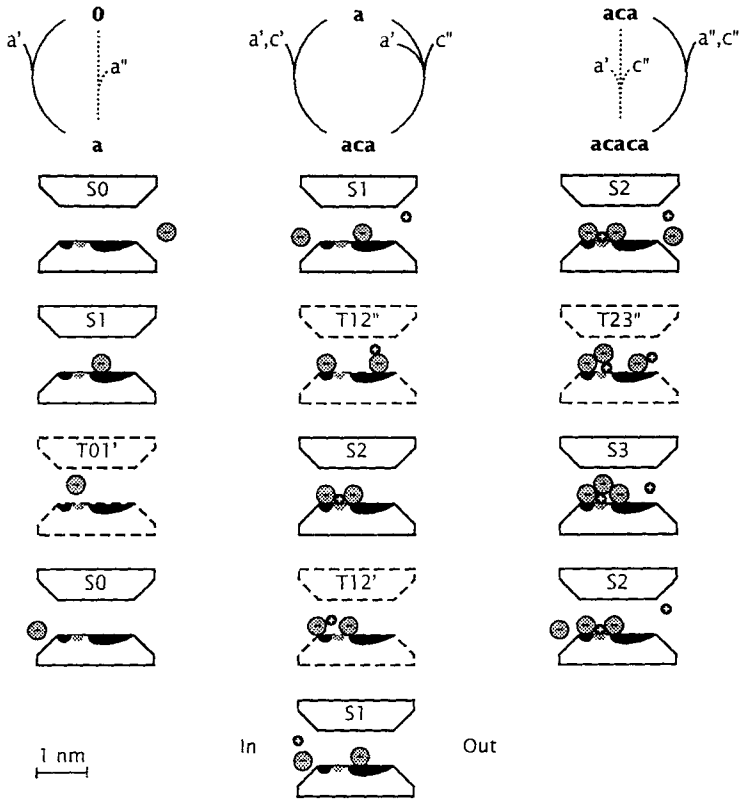

FIGURE 10. A molecular interpretation of Model E. Each column illustrates one of the three possible ion transport cycles (*top*) in the form of a dimensional sketch of the pore and the involved ions. Each top-to-bottom sequence corresponds to a clockwise walk through the transport cycle. Ions (Na and Cl) are scaled to their Pauling radii, and the narrow part of the pore is 0.7 nm in diameter (as needed for the largest known permeant ion) and 1.5 nm in length. The intracellular mouth of the pore is facing to the left. State labels match those of Table I, and transition states are shown in dashed outlines. Ion charges and presumed polar linings of the pore are highlighted by gray (−) or black (+) shades. The positions of ions in the pore correspond to the fitted charge parameters listed in Table I if the transmembrane electrical field drops linearly over the narrow stretch of the pore.

These sketches of the pore were dimensioned using the crystal radii of Na and Cl ion (0.95 and 1.81 Å), the minimal pore diameter determined with large anions and cations (0.7 nm), the charge parameters of model E (Table I), and the assumptions that state charges solely reflect ion positions and that electrical and geometrical

distances are equivalent. Recall that state charges in Table I are defined as the charge displaced when all ions are introduced through the intracellular mouth (see Methods).

The one-ion transport cycle, involving states S0 and S1, reveals the "internal profile" of the pore as probed by a single Cl ion. The anion dwells in a pore "site" where it senses 56% of the transmembrane voltage. Attraction to this site is fairly weak (corresponding to a k_D of 288 mM). Intracellular access to the site is limited by an "energy barrier" located about midway between the site and the inner pore mouth, whereas no comparable "barrier" exists on the extracellular side. Thus, the Cl ion appears to experience a favorable interaction with its environment in the exterior half of the pore and an unfavorable interaction in the interior half. Because of the wide diameter of the pore, these interactions might be electrostatic, as suggested by the shading pattern given to the pore lining in Fig. 10.

The charge parameter of the three-ion state, S2, is less negative than that of S1, although the net ionic charge (two anions and one cation) is the same. The arrangement proposed in Fig. 10 places the cation between the anions and in the internal (i.e., left) half of the pore. This allows one of the anions to dwell near the site used in S1, puts the cation into the location of the anion barrier of S1, and, with two ion locations determined, places the second anion near the inner mouth. An alternative, one anion in the S1 site and the other ions in the outer half of the pore, would place the second anion near the first and the cation beyond, which is electrostatically less plausible. Furthermore, the proposed arrangement conforms with the optimized model access rates: S2 is rapidly formed by accretion of an internal ion pair, whereas the acquisition of an internal Cl and external Na occurs at a slower rate.

The optimization of the kinetic model attributed a slightly positive charge to the five-ion state, S3, although the net ionic charge of S3 is negative. This requires that a cation be located near the external mouth and that the other ions cluster towards the interior side. The arrangement proposed in Fig. 10, which gives a correct state charge, involves a cluster of three anions formed around one of the cations. This may appear as an electrostatically forced grouping, but in fact it is not. Packed at the spacing of a crystal, the four-ion cluster per se is electrostatically stable in a vacuum (due to the small radius of the Na ion). On the other hand, an anion approaching the three-ion cluster (S2) is repelled until it can interact at close range with the cluster's Na ion. Fig. 10 shows that in the proposed S3 ion arrangement, the second Na ion can assist in the formation of the four-ion cluster. Overall, the vacuum electrostatic interactions would slightly favor the five-ion cluster proposed for S3 over the three-ion cluster of S2.

The sketches in Fig. 10 do not include water molecules, but it is clear that there is ample space between ions and pore walls that needs to be filled. The enthalpies of the crystal and solvated forms of NaCl differ only by 0.9 kcal/mol (~ 1.6 kT). Thus, small NaCl aggregates can readily form in an aqueous pore if ions are either packed together at crystal intervals or are spaced at intervals that allow for interspersed water molecules (e.g., between the single-cation and four-ion cluster in S3). This is borne out by the model parameters: the salt activities necessary to make the likelihoods of

the single-, three-, and five-ion states equal to that of the empty state are similar: 288 mM (S1), 377 mM (S2), and 360 mM (S3).

The length of 1.5 nm indicated in Fig. 10 for the narrow part of the pore implies that the ions forming a cluster are in direct contact to one another. A larger length would result if water molecules were intercalated between the ions of the proposed clusters, which might be possible because of the 0.7 nm minimal width of the pore. Intercalated water molecules would restrict the postulated ionic rearrangements only if their dynamics were substantially slower than exchange rates determined for inner ion shells in free solution. The postulated ion clusters were aligned with the long axis of the pore. Partially transverse alignments, which might be possible in a 0.7 nm wide pore, would result in a smaller estimate of the pore length.

Predicted Physiological Characteristics

Ionic conditions close to those in vivo and a voltage close to the resting potential do not permit direct observations of Cl single-channel currents. The elevated salt concentrations used in this study produce currents large enough to be observed, but these currents include a significant contribution of Na ion. As has been pointed out previously (Hille, 1992), a channel with a Na:Cl permeability ratio of 0.2 could not support a membrane potential more negative than ~ -45 mV. Our model derived from measurements at elevated salt concentrations, however, has features that could render the physiological Na permeability very small. In the model, Na influx requires three ions to form a complex, which becomes unlikely at low salt concentrations (single and triple occupancies become equally likely at ~ 300 mM). This complex includes a Cl ion recruited from the intracellular saline, where Cl activity is physiologically low. Finally, Na entry is not favored by negative potentials as the main barrier for Na ion is near the extracellular mouth.

Fig. 8 *C* shows model zero-current potentials computed for two experiments. In the first, internal Cl activity (abscissa) is reduced by substitution with an impermeant anion from 100 to 4 mM (cation: Na) while the external NaCl activity is maintained at 100 mM. In the second experiment, internal NaCl activity is increased from 100 mM to 1 M whereas, as before, external NaCl activity is constant at 100 mM. For internal Cl substitution, the zero-current potentials computed for Model E (*solid curve*) are virtually indistinguishable from the Nernst potentials for Cl (*dashed line*). Because Na and K ions are virtually not distinguished by the channel (Franciolini and Nonner, 1987), this prediction also applies to the physiological situation. By contrast, a sharp transition towards a limited cation/anion selectivity is predicted when the internal NaCl activity is increased above 100 mM.

The narrowly optimized cation rejection of this Cl channel might be a necessary consequence of the mechanism by which the channel selects for its physiological anion. The neuronal background channel, like many other Cl channels (reviewed by Hille, 1992), appears to rely on the lyotropic effect in selecting among physiological anions. The lyotropic effect usually implies an electrostatic interaction with a weak dipole and a hydrophobic interaction (cf. Dani, Sanchez, and Hille, 1983). If the pore were guarded by stronger positive groups, it likely would attract other physiological anions, such as intracellular polyvalent anions. In the absence of a strong electrostatic guard, however, the rejection of small alkali cations also becomes dependent on the

lyotropic effect. This rejection breaks down when alkali cations become attracted into the channel by bound anion. The breakdown would be sharply concentration dependent, as it requires the adsorption of several ions. It appears that a relatively low affinity for the physiological anion and relatively low salt activity are necessary for a cation/anion selectivity based on the lyotropic effect. Even though elevated salt activity enhances anion current in a hyperlinear fashion, it compromises cation rejection to a substantial degree.

APPENDIX

This section describes the computational method by which we optimized kinetic models of ion permeation. The method greatly reduces numerical stability problems inherent to commonly used curve-fitting methods and thus, is of possible general interest.

Optimization of Models

To distinguish between many possible kinetic schemes that might represent the multi-ion behavior of the Cl channel, we needed an efficient computational technique that allowed us to compare the capabilities of models to account for the experimental i/V relationships. As a criterion, we sought to determine the minimal sum of squares of the residuals between theoretical and experimental unitary currents. The search necessarily encountered models for which not all parameters could be determined from the available data. An ideal technique would indicate which parameters were essential and would optimize them while keeping nonessential parameters within a computationally safe range. Conventional optimization techniques do not do this. In particular, if some parameters of a model have either little or similar effects on the function of interest, the Gaussian least-squares method generates normal equations that have a singular or numerically near-singular coefficient (Hessian) matrix. Direct solution of these equations by standard numerical methods results in numerical overflow or very large and unstable corrections to some of the parameters. These parameter changes either have no effect on the function, or are delicately balanced by changes occurring in other parameters (this happens in permeation models, for example, when some configurations are visited with low probabilities).

One approach to stabilize the Hessian matrix is to scale up the elements of the main diagonal. This is done in the Levenberg-Marquardt method, which effects a graded transition between the Gauss and steepest-descent optimization methods. The Levenberg-Marquardt method proved inefficient for our purpose, because it stalled in small-step steepest-descent searches when major corrections to parameters were needed.

We therefore used a numerical method that directly addresses the problem of Hessian matrix singularity: singular value decomposition (SVD). This algorithm permits one to determine the system of orthonormal basis vectors that define the actual range of the matrix. The normal equations then can be solved using only the basis vectors of the range. For a detailed description of the algorithm and a discussion of its application in linear least-squares optimization see Press, Teukolsky, Vetterling, and Flannery, 1992, pp. 59–70 and 676–679). Here, we applied SVD to

solving the normal equations of a nonlinear problem. The algorithm was numerically stable and was robust in the sense that poorly determined parameters were stabilized near their assigned initial values or near useful values established in preceding iterations.

The normal equations were constructed from data comprising the experimental i/V relationships for several or all of the ionic conditions reported here. These relationships were fit simultaneously in one parameter optimization. The partial derivatives of unit current with regard to the parameters were computed from function differences spanning an interval of 0.002 to 0.02 (logarithmic) parameter units. Following SVD of the Hessian matrix (function 'svdcmp' in Press et al., 1992), rows whose corresponding singular values were smaller than an adjustable threshold (between 10^{-3} and 10^{-5} times the largest singular value) were discarded. The remaining underdetermined system was solved through an algorithm (function 'svbksb' in Press et al., 1992) that yielded a solution vector of minimal length. This vector either satisfied the normal equations or at least minimized the length of the vector of residuals.

The parameter corrections computed in this way were conservative in that they represented the smallest corrections that satisfied the normal equations. Nevertheless, since the normal equations were computed using first-order extrapolations of a nonlinear function, the corrections could overshoot their optimal values. Hence, the sum of squares was determined first with the full corrections. If this sum was not smaller than that from the previous iteration, the parameter corrections were reduced threefold, and a new test of the sum of squares was performed. If three consecutive reductions did not lead to an improvement of the fit, the threshold for rejecting rows with small singular values was increased twofold, and the normal equations were reevaluated. If the iteration yielded a reduction of the sum of squares, the singular value threshold was reduced twofold for the next iteration. If an iteration failed, a new attempt was made after adding small random variations to the parameters.

Optimization was started from initial parameter values obtained through a combination of guessing and experience with preceding models. The SVD-enhanced Gauss algorithm accepted crude initial parameters and generated substantial improvements within a few passes. Pivotal iterations on subsets of parameters were not useful. Models with up to 24 free parameters were optimized without encountering numerical problems, although all floating point computations were done in single precision (24 mantissa bits). Although exceptionally stable, the method did not safeguard against convergence problems due to local minima, which can occur in nonlinear optimization. Such problems arose when a model had sufficient complexity to produce a set of observations in several different ways. Therefore, we started from simple, rather than general, schemes and explored additional features in a step-wise fashion.

During an optimization, the singular values of the Hessian matrix were monitored. Typically, an order-of-magnitude break occurred after a certain number of large singular values. The singular value threshold chosen by the algorithm usually effected rejection of vectors with singular values below this break point. The rank of the remaining matrix did not exceed values of 10 to 14 in any tested model, indicating

that, regardless of the total number of free parameters, the experimental data were determined by no more than 10 to 14 independent parameters (generally not mapping one-to-one onto actual parameters). Iteration was terminated by intervention after parameters started to fluctuate about stationary values without significant further reduction of the sum of squares.

Assessment of Parameter Reliability

Since the nonlinear least-squares method could converge to a local, rather than general, minimum, optimizations of a model were performed from several different sets of initial parameters. The optimizations of most models converged to sums of squares that were similar within a few percent, indicating that the detected minimum was general within the range of physically reasonable parameters. When multiple minima were encountered, they were found to be due to redundant features of a model; the effects of these features were studied individually in simpler models.

Whereas our method was numerically stable with weakly determined parameters and indicated the number of reliable parameters by the singular values, it did not identify weak and strong parameters (or parameter correlations) directly. Parameters of models considered in detail were tested by deliberately adding random values between ± 1 kT or logarithmic charge unit and reoptimizing. The algorithm did not optimize ineffective parameters; these retained values close to their random initial settings and could be recognized in scatterplots of repeated parameter optimizations (see, e.g., Fig. 9 *A*).

In addition to these controls, we sought to establish confidence limits using a Monte-Carlo bootstrap method (cf. Press et al., 1992, chapter 15.6). Synthetic data sets were created by randomly drawing copies of i/V points from the pooled experimental i/V relationships. This yielded sets equal in size to the original, in which on average 37% of the original samples were replaced by duplicates of other samples. A parameter optimization was performed for each synthetic data set. Scatterplots of these parameters (see, e.g., Fig. 9 *B*) yielded estimates of the parameter distributions and revealed parameters that were sensitive to the outcome of particular measurements.

We thank Dr. Ellen Barrett for commenting on the manuscript. This work was supported by grant GM-30377 by the National Institutes of Health.

Original version received 20 January 1994 and accepted version received 24 May 1994.

REFERENCES

Begenesich, T. B., and M. D. Cahalan. 1980. Sodium channel permeation in squid axons. I. Reversal potential experiments. *Journal of Physiology.* 307:217–242.

Blatz, A. L. 1991. Properties of single fast chloride channels from rat cerebral cortex neurons. *Journal of Physiology.* 441:1–21.

Borisova, M. P., R. A. Brutyan, and L. N. Ermishkin. 1986. Mechanism of anion-cation selectivity of amphotericin B channels. *Journal of Membrane Biology.* 90:13–20.

Dani, J. A., J. A. Sanchez, and B. Hille. 1983. Lyotropic anions. Na channel gating and Ca electrode response. *Journal of General Physiology.* 81:255–281.

Franciolini, F., and W. Nonner. 1987. Anion and cation permeability of a chloride channel in rat hippocampal neurons. *Journal of General Physiology.* 90:453–478.

Franciolini, F., and W. Nonner. 1994. Anion-cation interactions in the pore of neuronal background chloride channels. *Journal of General Physiology.* 104:711–723.

Hille, B. 1992. Ionic Channels of Excitable Membranes. Second edition. Sinauer Associates Inc., Sunderland, MA.

Hille, B., and W. Schwarz. 1978. Potassium channels as multi-ion single-file pores. *Journal of General Physiology.* 72:409–442.

Naranjo, D., and R. Latorre. 1993. Ion conduction in substates of the batrachotoxin-modified Na^+ channel from toad skeletal muscle. *Biophysical Journal.* 64:1038–1050.

Naranjo, D., R. Latorre, D. Cherbavaz, P. McGill, and M. F. Schumaker. 1994. A simple model for surface charge on ion channel proteins. *Biophysical Journal.* 66:59–70.

Press, W. H., S. A. Teukolsky, W. T. Vetterling, and B. P. Flannery. 1992. Numerical Recipes in C. Second edition. Cambridge University Press, Cambridge, MA.

Robinson, R. A., and R. H. Stokes. 1965. Electrolyte Solutions. Second edition. Butterworths, London. 492 pp.

Zambrowicz, E. B., and M. Colombini. 1993. Zero-current potentials in a large membrane channel: a simple theory accounts for complex behavior. *Biophysical Journal.* 65:1093–1100.